JOURNAL OF PROPULSION AND POWER
Vol. 12, No. 1, January–February 1996

Dual Stream Axisymmetric Mixing in the Presence of Axial Vorticity

V. M. Belovich,* M. Samimy,† and M. F. Reeder‡
Ohio State University, Columbus, Ohio 43210

An experimental investigation was undertaken to study mixing in a coaxial jet where the inner nozzle is a lobed mixer. Four inner jet nozzle geometries were explored: a baseline circular jet and three different six-lobed nozzles. Also, three velocity ratios of 3:1, 1:1, and 1:3 (inner:outer) were examined. Flow visualizations using a passive scalar were performed using a laser sheet from a Nd:YAG laser. The laser has a 9-ns pulse duration that effectively freezes the flow. Instantaneous cross-sectional images were taken as well as streamwise views. The effects of various parameters such as the interfacial area increase due to the lobed nozzle geometry, the strength of streamwise vortices, and the large-scale structures on the mixing process are evaluated and discussed. Results showed highly enhanced mixing as the strength of the streamwise vortices increased. In addition, the presence of large-scale structures due to the Kelvin–Helmholtz instabilities, and their interaction with streamwise vortices generated by the lobes were found to be crucial for enhanced mixing. The fraction of mixing enhancement due to streamwise vorticity (relative to mixing enhancement due to increased interfacial contact area) was found to increase as velocity ratio increased. This fraction also increased with downstream distance.

Nomenclature

C = constant
D = nominal diameter of the baseline nozzle, 1 in.
h = lobe height
L = lobe length
U_{ref} = reference axial velocity
α = lobed nozzle ramp angle
Γ = circulation
λ = wavelength of laser light

I. Introduction

MIXING is an important phenomenon in all combustion systems from low-speed systems such as coal-fired boilers, oil- and gas-fired furnaces, and gas-turbine engines, to high-speed systems such as scramjets and flows through nozzles of supersonic aircraft. A critical technical problem to be solved in many of these applications is the mixing between two gaseous streams. How quickly and how well a fuel and oxidant can be mixed will have a major influence on the combustion efficiency, heat release rate, pollutant formation, combustor size, and many other critical parameters. Vorticity dynamics greatly impact the mixing process. The streamwise vortices generated in a flow, in addition to the spanwise (in planar shear layers) or ring-type (in axisymmetric shear layers) vortex roll-up processes, have been found to mix fluid streams quickly and efficiently. Generating these vortical structures using a lobed mixer and investigating the nature of these structures and their mixing enhancement capabilities are the subject of the present study.

Presented as Paper 94-3084 at the AIAA/ASME/SAE/ASEE 30th Joint Propulsion Conference and Exhibit, Indianapolis, IN, June 27–29, 1994; received Aug. 12, 1994; revision received Feb. 9, 1995; accepted for publication March 29, 1995.

*Graduate Student, Department of Mechanical Engineering. Member AIAA.

†Professor, Department of Mechanical Engineering. Associate Fellow AIAA.

‡Graduate Student, Department of Mechanical Engineering; currently National Research Council Fellow, NASA Lewis Research Center, Cleveland, OH 44135. Member AIAA.

The lobed mixer produces streamwise vortices (e.g., Paterson[1,2] and Povinelli et al.[3]) on the order of the nozzle dimensions. These relatively large-scale streamwise vortices aid the mixing process by entraining additional fluid from the secondary stream into the mixing layer, and conversely, sweeping the primary flow into the secondary stream.

Most of the early studies[3–14] of lobed mixers were greatly influenced by the gas-turbine industry, as many of the test configurations were scale models of turbofan engine exhaust sections. The geometry consisted of a central solid body around which flowed the hot core fluid with the bypass air surrounding the core. The lobed mixer was an axisymmetric shape separating the two fluid streams. Among the significant findings of these studies was that lobed mixers were found to generate streamwise vorticity more efficiently (i.e., with less pressure drop) than the conventional methods, and thus, provided an engine performance improvement. Another important benefit of lobed mixers is that their improved entrainment reduces the velocity of the high-speed exhaust gases, thereby reducing noise. Other findings include scalloping the lobes aids in mixing and that lobe penetration in the fluid streams has the most significant effect on mixing effectiveness, as long as the flow does not separate. Separation increases the pressure losses and decreases mixing effectiveness.

Paterson[1,2] studied subsonic flow issuing from a lobed nozzle for both cold and heated flows. Detailed pressure and temperature data were taken, as well as three-dimensional laser Doppler velocimetry (LDV) measurements. Paterson found that large-scale secondary flows, set up by the nozzle, produced streamwise vortices of low intensity with a length scale on the order of the nozzle radius. Also, a horseshoe vortex on the order of the lobe half-width was found to exist in the lobe troughs. The contribution to the overall mixing process of each was not clear, but the secondary flow vortices were expected to be dominant because of their much greater size. The lobed mixer was found to rapidly mix flows at large scale.

Much of the later work on lobed mixers concentrated on discovering the underlying physics of the lobed mixing process by using a two-dimensional lobed mixer, which is essentially a corrugated plate. Werle et al.[15] found that the vortex formation process was an inviscid one. Also, the mixing process was proposed to take place in three basic steps: 1) the vortices

form, 2) intensify, and 3) then rapidly break down into small-scale turbulence. In effect, the lobed mixer was thought to act as a fluid stirrer initially to mix the flow, until the vortices broke down to produce small-scale mixing.

Other studies during the last 10 years or so tested the performance of lobed mixers in applications such as ejectors,[16,17] supersonic flow,[18,19] and in combustion.[20,21]

Eckerle et al.[22] used two-component LDV to study mixing downstream of a lobed mixer at two velocity ratios. They determined that the breakdown of the large-scale vortices and the accompanying increase in turbulent mixing are important parts of the mixing process. It was also shown that this vortex breakdown occurs further upstream for a velocity ratio of 2:1 rather than for 1:1.

Barber et al.[23] studied three different two-dimensional lobed mixers both analytically and experimentally. Performing a one-dimensional inviscid analysis to predict lobe circulation and geometrical scaling relations produced results in reasonable agreement with their data, further emphasizing the inviscid nature of the overall large-scale mixing process. Circulation was found to scale well according to the following relation:

$$\Gamma \propto CU_{\text{ref}}(h^2/L)$$

For a straight-contour (in the axial direction) lobe, α can be related to h/L by the inverse tangent function. Thus, circulation is proportional to ramp angle. One of the conclusions of the study was that lobed mixers with parallel side walls produce higher streamwise circulation than lobes with sinusoidal or triangular shapes. The close proximity of the walls in the lobe peak region for the latter shapes creates thicker boundary layers that reduce the effective lobe height, and therefore, reduce circulation. In addition, lobes with sinusoidal and triangular shapes have a theoretically lower value of C in the previous equation. The lobes for the nozzles of the present study have a radial geometry. That is, the sides of the lobes are directed along radii, and thus, the lobe width increases away from the axis centerline.

Mixing downstream of a lobed mixer is controlled by three primary elements. The first element is the increased interfacial area between the two fluid streams because of the convoluted trailing edge of the nozzle. The second is the streamwise vorticity generated due to the alternate inwardly and outwardly angled flow paths of the air through the nozzle. The third is the Brown–Roshko-type structures that are generated in any free shear layer with velocity gradients across the layer, due to the Kelvin–Helmholtz instabilities. Manning[24] attempted to separate the effects of these three mechanisms in two-dimensional water-tunnel experiments. He studied a flat plate, for use as a baseline case, and two different lobed mixers, one of which had a convoluted, yet straight (i.e., no ramp angle) extension section to damp the streamwise vorticity. It was shown that the mixing performance of the lobed mixer exceeds the performance of the convoluted plate by an amount that increases as velocity ratio increases. Also, at velocity ratios close to 1, the increased mixing is due mainly to the increased contact area, whereas the streamwise vorticity has the larger role at a velocity ratio of 2. Manning's and other work from MIT are summarized in Elliott et al.[25]

A very detailed and systematic study by McCormick[26] revealed more details of the flow patterns downstream of a lobed mixer. Extensive flow visualizations for laminar and turbulent airflow, and three-dimensional velocity measurements taken with a hot-wire, showed that the interaction of Kelvin–Helmholtz (normal) vortices with the streamwise vortices produces the high levels of mixing. The streamwise vortices pinch off the normal vortices, thus, enhancing the stirring effect in the flow. This pinching causes the normal vortices to merge within 1.5 lobe heights downstream, where they were observed to break down shortly thereafter, leading to intense turbulent mixing. Another interesting observation by McCormick is that the scale of the normal vortices shed from the lobed mixer is about one-fourth that shed from a planar baseline case. From this McCormick and Bennett[27] infer that the lobed mixer introduces smaller scales into a flow sooner, which may also enhance small-scale mixing.

Presz et al.[28] studied axisymmetric, lobed mixers used in ejector applications. They found that an aggressively designed mixer, having ramp angles of 45-deg inward, 30-deg outward, and scalloped lobes, produced pumping performance approaching ideal values. Scalloping the lobes has also been used before with success.[10] The study of Presz et al. is significant to the present work because it is a return to the original axisymmetric designs of the 1970s and early 1980s, but with a significant difference. The difference is that the earlier work had a centerbody that was used to represent the core/shaft of the jet engine. The centerbody, in effect, created an inner annular flow (hot core flow), surrounded by the lobed mixer nozzle that separated it from the outer annular flow (bypass or fan flow). In essence, two annular flows were being mixed. Similarly to the experiments of Presz et al.,[28] the present study uses the lobed mixer as a central (convoluted) jet, which then mixes with an outer (annular) flow. By varying the velocity ratio of inner flow to outer flow as well as the nozzle geometry, the three primary elements that affect mixing with lobed nozzles were studied. The present study parallels that of Manning[24] in many ways. However, that work was concerned exclusively with two-dimensional mixing layers and very low Reynolds number.

II. Experimental Facility and Techniques

A. Facility

The experiments for this work were conducted at the Aeronautical and Astronautical Research Laboratory at the Ohio State University. The air supply for the tests is provided by two four-stage compressors and is stored in two tanks of 42.5-m^3 (1500-ft^3) volume at pressures up to 16.9 MPa (2450 psi). The air is throttled through two valves, piped through 2-in. steel pipe and separated into two branches through a tee section. One branch supplies the primary (central) flow, the other supplies the secondary (outer) flow. Downstream of the tee are two ball valves used for regulating the inner and outer flows to the test sections. The flow rates to the primary and secondary streams are measured so that the desired average exit plane velocities can be set. The flow rates are metered using Dwyer model DS-200 flow sensors that are averaging pitot probe devices and require the measurement of differential and static pressures. The differential pressures are measured using a Dwyer model 422-23 incline manometer (0.02-in. water per division) for the central flow and a Dwyer model 1230-16 U-tube manometer (0.1-in. water per division) for the outer flow. At high flow rates, a mercury manometer (0.1-in.Hg per division) is used for the outer flow. Calibrated gauges are used for the static pressure measurements.

Figure 1 shows a schematic drawing of the settling chamber and the contraction section. The primary flow enters through a single central tube while the secondary flow enters through two separate bottom inlets. The secondary air is forced to exit radially into the settling chamber through a wire screen at each inlet. The flow then passes through a 25% open perforated plate and two 51% open perforated plates to reduce the turbulence level and flatten the velocity profiles. The contraction section is smoothly contoured (fifth-order polynomial) with a 7.44 to 1 area ratio and an exit diameter of 63.5 mm (2.5 in.). The end piece of the outer nozzle is 2 in. long and constructed out of Plexiglas®. The system was designed to allow for a wide range of primary and secondary flow rates and velocity ratios. Velocities at the exit up to 120 m/s can easily be maintained in either the primary or secondary flows.

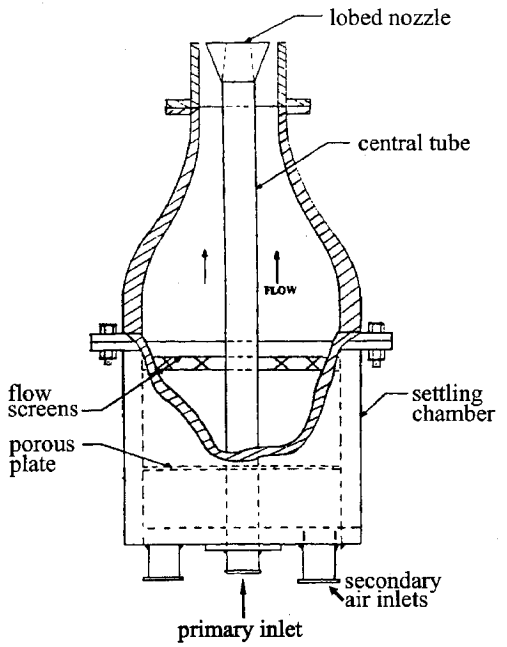

Fig. 1 Schematic of settling chamber and contraction section.

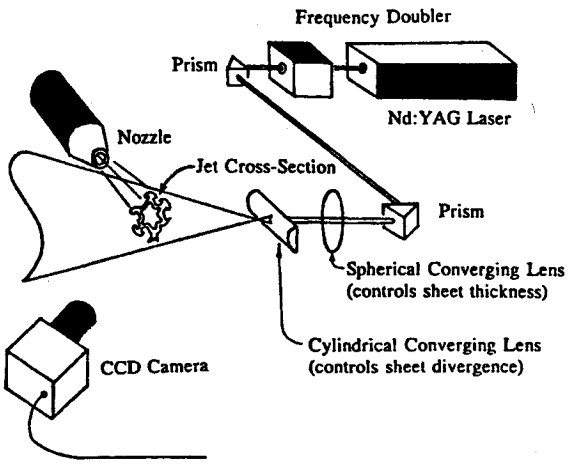

Fig. 2 Optical setup for flow visualizations.

Tobacco smoke was injected upstream of the stagnation chamber into the primary stream. The smoke patterns were illuminated using a Quanta Ray GCR-4 frequency doubled (λ = 532 nm) Nd:YAG laser. The Nd:YAG laser is capable of producing 600 mJ at 532 nm and has a pulse rate of 10 Hz with a 9-ns duration, effectively freezing the flow. A Princeton Instruments 14-bit intensified charged coupled device (CCD) camera, synchronized with the laser, was used to record the images, which were then stored on a personal computer. The optical setup is shown in Fig. 2. The laser beam is directed to the test section using prisms and focused into a laser sheet approximately 0.5 mm thick. The orientation shown in the figure is for cross-sectional views. The optics were also set up so that streamwise images could be recorded.

B. Nozzle Design

Several lobed mixer nozzles have been designed, having both four and six lobes. However, only the results for the six-lobed nozzles will be presented here. Photographs of the baseline nozzle and the six-lobed nozzles are shown in Fig. 3. The baseline nozzle was manufactured from thick wall stainless steel tubing with a nominal 1-in.-diam o.d. The inside surface was machined to produce a wall thickness of 0.75 mm (i.d. = 23.9 mm), which matches the thicknesses of the lobed nozzles.

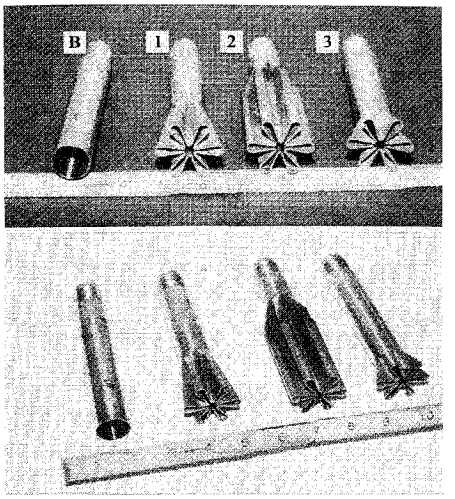

Fig. 3 Views of the baseline circular nozzle and six-lobed nozzles. From left to right they are: baseline circular NB, nozzle 1 (10 deg), nozzle 2 (0 deg), and nozzle 3 (20 deg).

The lobed nozzles were manufactured from stainless-steel bar stock by wire electron discharge machining. Manufacturing a nozzle with a thinner wall would require annealing the bar stock prior to cutting. The exit areas of the baseline nozzle and the lobed nozzles are approximately 450 mm^2. The nozzle outlet geometries are constructed of circular arcs connected with straight lines that are directed radially outward. The total lengths of all the nozzles are 152.4 mm. The nozzles are silver-soldered onto the stainless-steel tube section and excess solder is filed smooth to the touch, both inside and out. Nozzle 1 has inward and outward ramp angles of 10 deg. Nozzle 2 has the same cross section as nozzle 1, but has a ramp angle of 0 deg. The straight, yet convoluted, section is used to damp out the streamwise vorticity (the circulation of the streamwise vorticity scales with ramp angle). Comparing nozzle 2 with the baseline nozzle, the effect of increased interfacial contact area can be separated, since the exit perimeter is much greater for nozzle 2. Comparing nozzles 1 and 2, the effect of adding streamwise vorticity to the flow can be quantified, since the interfacial contact area is the same for both. Nozzle 3, with ramp angles of 20 deg, is designed to produce the highest level of streamwise vorticity for the nozzles tested. The geometric parameters of the nozzles are summarized in Table 1. Each nozzle was tested under five different flow conditions, summarized in Table 2. Only three of these conditions are reported here: the 30:10, 30:30, and 30:90 m/s (inner:outer) flow conditions.

Flow visualizations for a preliminary test nozzle in the present investigation showed a high degree of flow separation for a nozzle with an outward ramp angle of 20 deg and an inward ramp angle of 10 deg, which produced a moderate 15% increase in cross-sectional area over its 1.25-in. length. Therefore, the nozzles used in the present investigation were designed to maintain constant cross-sectional area.

III. Results and Discussion

Figure 4 shows averages of 50 instantaneous cross-sectional images taken at three different locations downstream for the baseline nozzle and the six-lobed nozzles, at a velocity ratio of 3:1 (inner:outer). In this and the following two figures, the nozzles are arranged in order of increasing streamwise vorticity, from top to bottom. D is the diameter of the baseline nozzle (approximately 1 in.). The baseline nozzle shows the expected spreading downstream that is typical of round jets. The lobed nozzles show spreading, at a higher rate. Nozzle 2 at x/D = 1, shows smoke from six distinct lobes. By x/D = 2, the individual lobes are still distinct, however, they have

Table 1 Nozzle geometries

Nozzle	Description	Length of nozzle, mm	Ramp angles, deg	Exit area, mm^2	Exit perimeter, mm
Baseline	Circular	NA	NA	448	75
1	Six lobes, long	50.8	9.6/10	453	246
2	Six lobes, straight	76.2	0/0	453	246
3	Six lobes, short	25.4	19/20	453	245

Table 2 Operating conditions

Operating condition	V_{inner}, m/s	V_{outer}, m/s	$V_{pri}:V_{sec}$
1	30	10	3:1
2	30	30	1:1
3	30	90	1:3
4	90	30	3:1
5	90	90	1:1

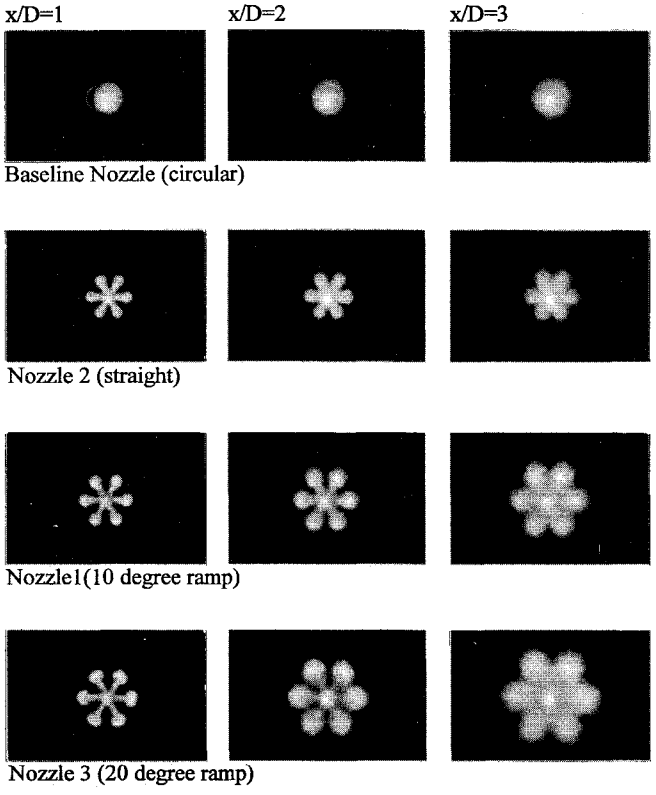

Fig. 4 Effect of adding streamwise vorticity for a velocity ratio of 30:10 m/s (inner:outer).

each grown thicker in addition to growing radially outward. By $x/D = 3$, only the tips of the lobes are noticeable, since adjacent lobes have merged. The spread of the smoke for nozzle 2 is greater than for the round jet considering that they have equal exit areas.

Nozzle 1 (10-deg ramp angle) in Fig. 4 shows similar behavior to nozzle 2, but the spread of the jet has improved due to the addition of streamwise vorticity. For nozzle 3, the changes are even more dramatic. Not only do the individual lobes spread more rapidly, but the entire jet spreads radially as well. Increasing the lobe angle, thus, increasing the strength of the streamwise vortices, clearly increases the jet spread. At $x/D = 1$, even these averaged images show the existence of counter-rotating streamwise vortices in the form of mushroom-shaped smoke concentrations toward the tip of each lobe for nozzle 1, and especially nozzle 3. This shows that the flow is fairly spatially stationary.

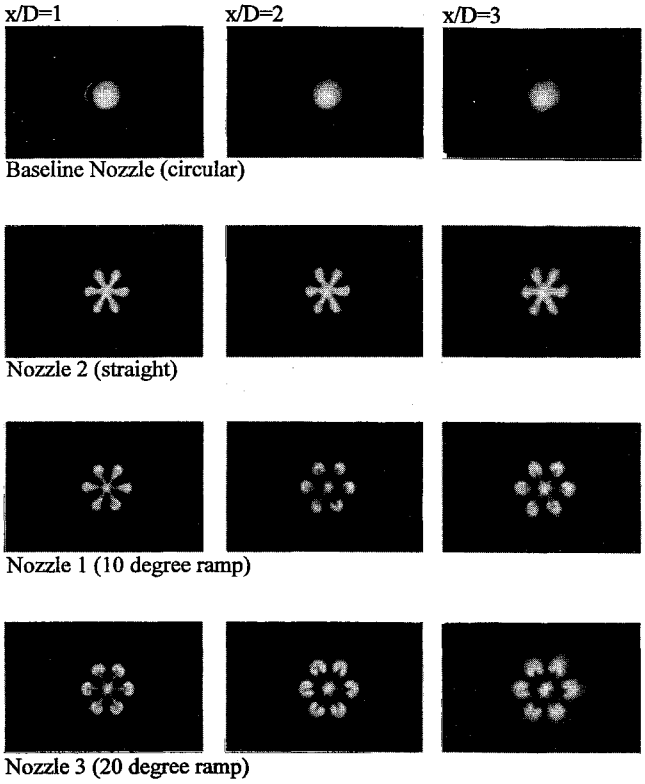

Fig. 5 Effect of streamwise vorticity at a velocity ratio of 30:30 m/s (inner:outer).

Images taken at the nozzle exit showed no evidence of flow separation for any of the nozzles, and so they are not presented here. Images at x/D locations farther downstream (e.g., $x/D = 5$ and 7) just show a more mixed cross section, and so they will not be shown either.

Figure 5 shows similar images to the previous figure except that the velocity ratio is now 1:1, i.e., 30 m/s for both inner and outer streams. This flow condition minimizes the Kelvin–Helmholtz instability, but cannot eliminate it completely because of the inner and outer boundary layers at the lobe peaks and nonparallelism of the flow due to the ramps. Nevertheless, the figures show that interface rollup is essentially eliminated. In all cases, the smoke from the individual lobes has not yet merged, and thus, the spread of the jet has been significantly reduced. There is still growth of the lobes and overall jet growth but no lobe interaction. With the Kelvin–Helmholtz roll-up minimized, the visualizations of the jet issuing from nozzle 1, and especially nozzle 3, clearly show the existence of streamwise vortices. At $x/D = 1$, the smoke begins to concentrate in the outer tips of the lobes, and at $x/D = 2$, it is turning radially inward towards the centerline. The clearly identifiable, smoke-filled, U-shaped regions at each lobe tip are indicative of two counter-rotating streamwise vortex pairs. The smoke at $x/D = 3$ has diffused even more, especially at the lobe tips. This could be due to the small Kelvin–Helmholtz effect at the lobe tips mentioned earlier and also to the pumping action of the streamwise vorticity.

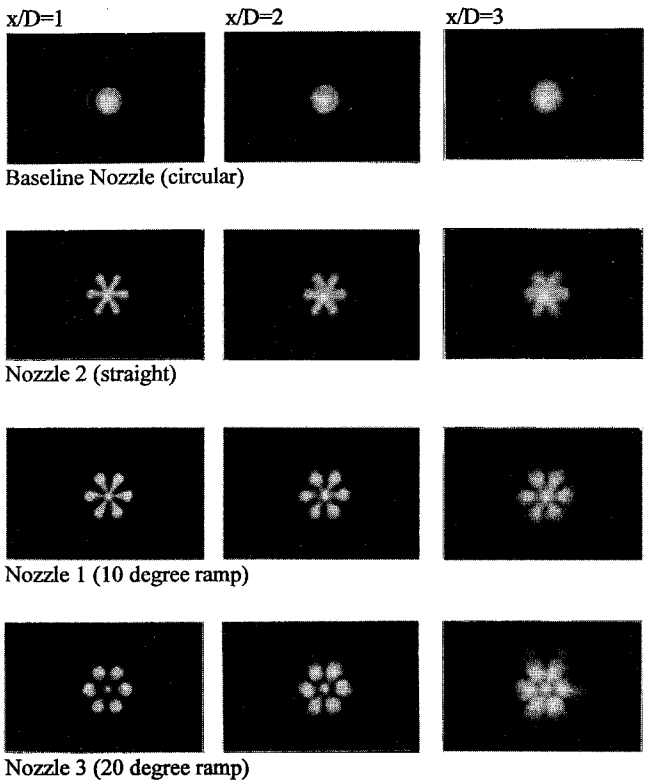

Fig. 6 Effect of streamwise vorticity for a velocity ratio of 30:90 m/s (inner:outer).

The results for the last velocity ratio of 1:3 (30:90 m/s, inner:outer) are shown in Fig. 6. Looking at the figure from left to right, it appears that overall jet spread is small for a given nozzle at various downstream locations and even less than for the 1:1 velocity ratio. The effect of adding streamwise vorticity is more apparent in terms of spreading of the individual lobes. However, this spreading does not appear to be enough to increase the overall jet spread. The instability characteristics of this case are quite different from the 3:1 case. This case is much more like a wake flow rather than a jet flow. Tennekes and Lumley[29] derived the spread of a self-preserving wake flow to be proportional to $x^{1/3}$, whereas a self-preserving jet spreads proportionally to x. Even though this flow is not self-preserving at these downstream distances, one would still expect a similar trend. (This difference will be more easily seen in the streamwise visualizations of Figs. 8–10.)

Figure 7 presents rms images for the baseline nozzle and nozzles 2 and 3 for all three velocity ratios at a single location downstream ($x/D = 3$). The rms is high (i.e., brighter) where the fluctuation in smoke concentration (or smoke intensity) is high. A low rms (i.e., darker regions) could indicate areas where the smoke is either well-mixed, not mixed (i.e., core flow), or where there is no smoke at all. The average images in the previous figures should be taken into account when interpreting this data. In any case, the regions of high rms (i.e., highly fluctuating smoke intensities) can be used to roughly define the intermittent mixing region, which is related to mixing by large-scale structures. Using this definition, for the circular nozzle, the mixing region forms a ring shape, as expected. For the velocity ratio of 3:1, the ring structure is well defined, with the inside of the ring being relatively dark. At the velocity ratio of 1:1, the mixing layer is also well defined, but occupies a much smaller area and is thinner. The final velocity ratio of 1:3 is similar to the others but shows that there is much more intermittency in the center part of the jet. The main mixing layer (i.e., ring) is slightly thicker than for the 1:1 case. Similar results can be seen for nozzle

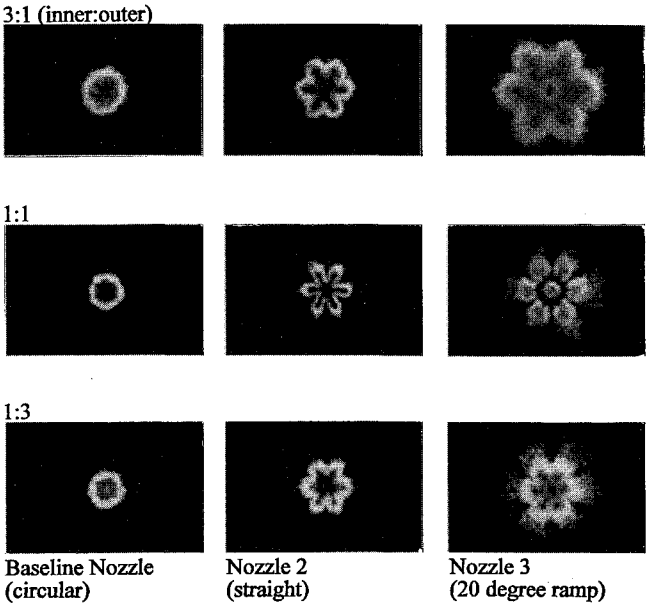

Fig. 7 Comparison of rms images at $x/D = 3$, showing effect of Kelvin–Helmholtz and streamwise vorticity.

2, i.e., the mixing layer for the 1:3 case is thicker than for the 1:1 case, but comparable to the 3:1 case. However, the overall spread of the jet for the 3:1 velocity ratio is higher than the two other cases.

For nozzle 3 the mixing layer does not form a continuous boundary around the nozzle for a velocity ratio of 1:1. The dark spot in the center of the image indicates very low intermittency. This indicates a very strong jet of smoke issuing from the centerline of the nozzle. Surrounding this dark spot is a ring of high intermittency at the location where the outer, unseeded flow is brought radially inward along the 20-deg inward ramp. Outside this ring is a dark ring of low mixing that matches the dark section of the average image previously seen in Fig. 5. In this region the smoke has been forced radially outward and the unseeded air is caught up in the counter-rotating vortex pairs, which effectively dilutes the smoke in this region. The outer, lobe-shaped mixing region of Fig. 7 encompasses the smoke-filled streamwise vortices shown in Fig. 5. The image for the 1:3 velocity ratio once again shows a continuous mixing layer surrounding the central flow and also shows more activity in the interior. The Kelvin–Helmholtz effect is more pronounced and smooths over the structures caused by the streamwise vorticity.

Figures 8 and 9 show streamwise views of instantaneous, average, and rms images for the baseline nozzle and nozzle 3, respectively. The average and rms images were calculated using 75 instantaneous images. The laser sheet was oriented vertically and passed through the centerline of the nozzle axis, aligned with the lobe tips. The flow is shown moving from left to right from approximately $x/D = 0$ to 8. The drop in intensity at the far right of the images is due to the Gaussian nature of the laser sheet. In Fig. 8, at a 3:1 velocity ratio, the jet spreads radially and the Brown–Roshko structures are angled upstream. At 1:1, the structures near the nozzle exit are smaller with a slight angle upstream. There appears to be a helical mode developing between x/D of 4–6. For the case where the outer flow is faster, a definite downstream angle to the structures can be seen, as expected. The average images show the relative spreading rates between the different velocity ratios. The spreading of the jet for the 1:3 velocity ratio begins similarly to the 1:1 case, but appears to be slightly higher further downstream. The rms images show the same general trends. The 3:1 velocity ratio case has an outwardly growing mixing layer, while the case with negligible Kelvin–Helmholtz rollup has very minor spread. On the other hand,

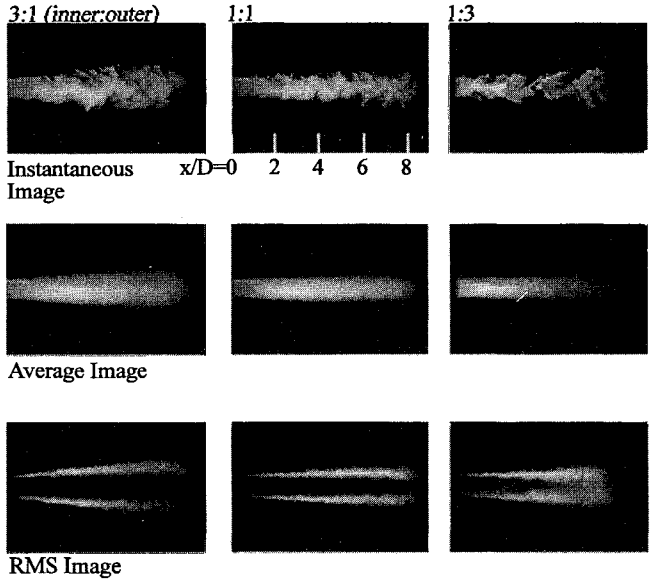

Fig. 8 Baseline nozzle comparison of instantaneous, average, and rms images.

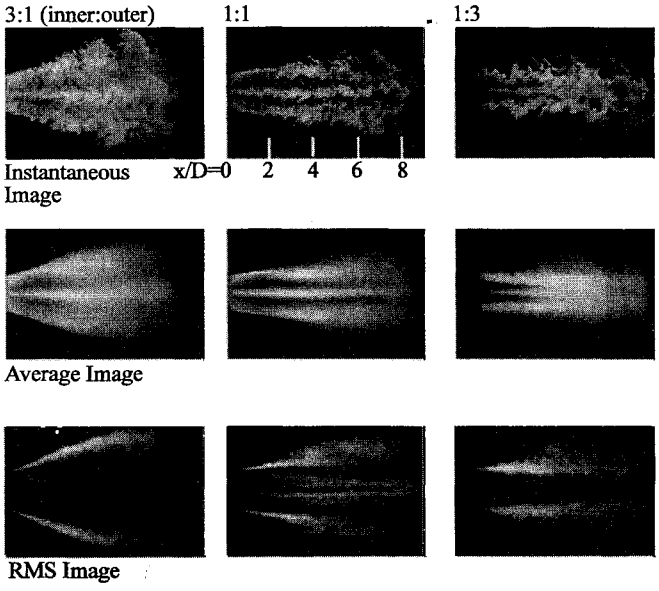

Fig. 9 Comparison between instantaneous, average, and rms images for nozzle 3.

the last case shows an inwardly growing mixing layer that eventually merges along the jet centerline, such that the potential core of the jet appears to end at approximately $x/D = 6$.

The three rms images in Fig. 8 exhibit flow patterns similar to those observed in previous coaxial jet studies.[30–32] Champagne and Wygnanski showed that the length of the inner potential core decreased as the inner to outer velocity ratio decreased. Figure 8 clearly shows that the 1:3 velocity ratio case has the shortest potential core length, as evidenced by the intermittent region filling the jet's central region by $x/D = 6$. This behavior was also seen in flow visualizations of low speed water jets by Dahm et al.[31] Other measurements taken by Champagne and Wygnanski[30] and by Ko and Au[32] show that the outer potential core (annular region) is longer than the inner core and that this length is independent of velocity ratio for $U_i/U_o < 1$. The development of the mixing layers in such coaxial jets is an intricate combination of shear layer and wake instabilities that are strongly coupled between inner and outer layers.[31]

Figure 9 displays similar results for nozzle 3 (20-deg ramp angle). The 3:1 velocity ratio case shows a significant spread relative to the baseline nozzle. The 1:1 and 1:3 ratio cases produce a sudden jump in jet growth rate across this plane (laser sheet oriented through nozzle peaks) at approximately $x/D = 3$, which is not noticeable in the instantaneous images. This jump could be indicative of a different instability characteristic. Another possible explanation is that because the lobed mixer acts as a fluid stirrer until the vortices break down,[15,22] and as the smaller scale, higher intensity mixing takes place, this breakdown is producing the jump in jet spread. This effect could also be related to the normal vortex pinch-off event seen by McCormick.[26] This issue requires further study.

Figure 10 compares streamwise average images for nozzles 1–3 at the three velocity ratios. Again, the flow is shown moving from left to right from approximately $x/D = 0$ to 8. The 3:1 velocity ratio case shows a higher jet spread with increasing streamwise vorticity from top to bottom. At a 1:1 ratio, there is little interaction between the smoke from the lobes and that exiting along the centerline of the nozzle, as evidenced by the black streaks separating the smoke-filled regions. This effect is not as prominent for nozzle 2 because the lobes of the straight section fill completely with smoke and the smoke does not get diluted by inwardly rushing, unseeded air, thus creating the dark streaks. When the velocity ratio is other than 1:1, the unmixed (black) streaks are thoroughly mixed by $x/D = 4$. These images also show that nozzle 1 produces a sudden jump in growth that is similar to the jump for nozzle 3 in Fig. 9.

To quantify the gross mixing of the inner jet with the outer jet, an estimate of the spread of the inner jet (smoke-marked area) was made. Every pixel intensity above a certain threshold was counted as part of the spread center jet, and those below the threshold were considered background. Plotting a histogram of the number of pixels vs pixel intensity for the average images was found to provide an adequate method for separating pixels representing smoke from pixels representing background intensity. For the majority of the images, the signal was readily apparent, forming a hump in the data at the higher end of the intensity scale. The other images (usually at the higher x/D values) did not have a readily discernible hump in the histogram, but exhibited a relatively flat portion followed by a dropoff at the higher intensities. The results are shown in Fig. 11. In this figure, the calculated area of the inner jet normalized by the exit area of the baseline jet is plotted vs x/D location for four different nozzles. The

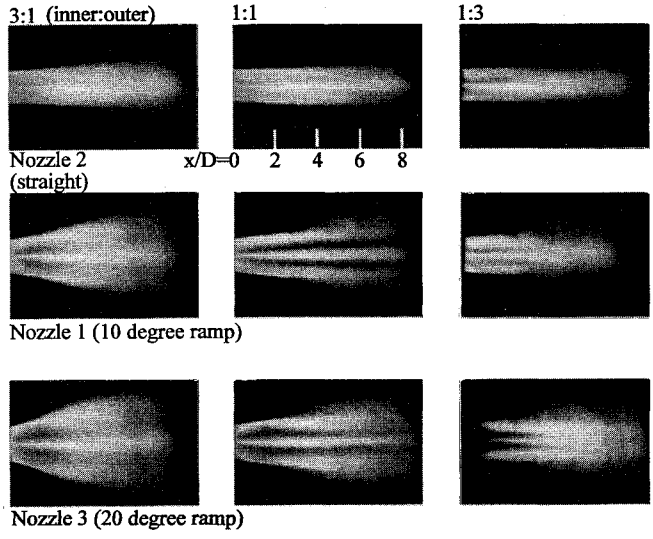

Fig. 10 Streamwise views of the three six-lobed nozzles for the three velocity ratios.

Table 3 Contributions to mixing by interfacial area and streamwise vorticity for nozzle 1

Velocity ratio	Contribution	x/D = 1, %	x/D = 2, %	x/D = 3, %
3:1	Interfacial area	40	39	32
	Streamwise vorticity	60	61	68
1:1	Interfacial area	73	58	37
	Streamwise vorticity	27	42	63
1:3	Interfacial area	72	63	52
	Streamwise vorticity	28	37	48

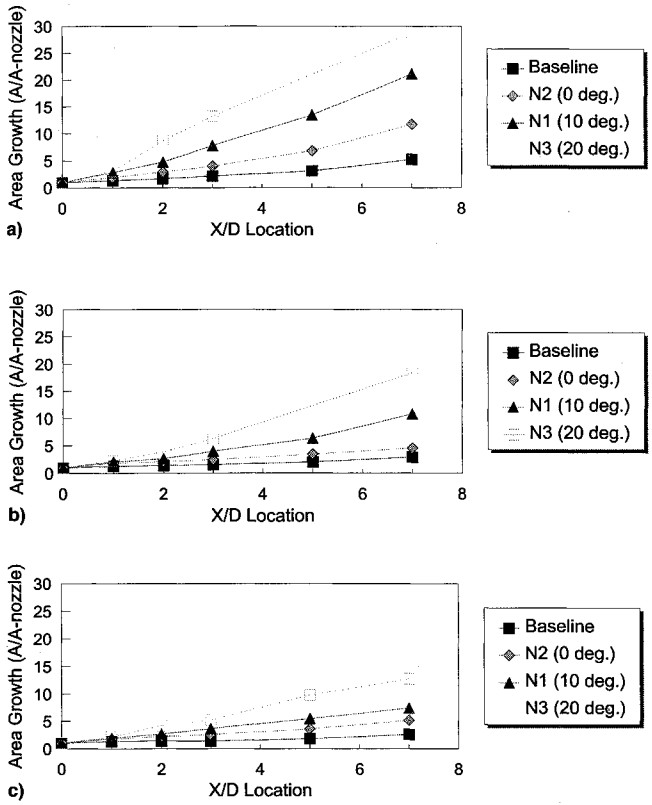

Fig. 11 Comparison of jet spread for the six-lobed nozzles: a) 3:1, b) 1:1, and c) 1:3 velocity ratios.

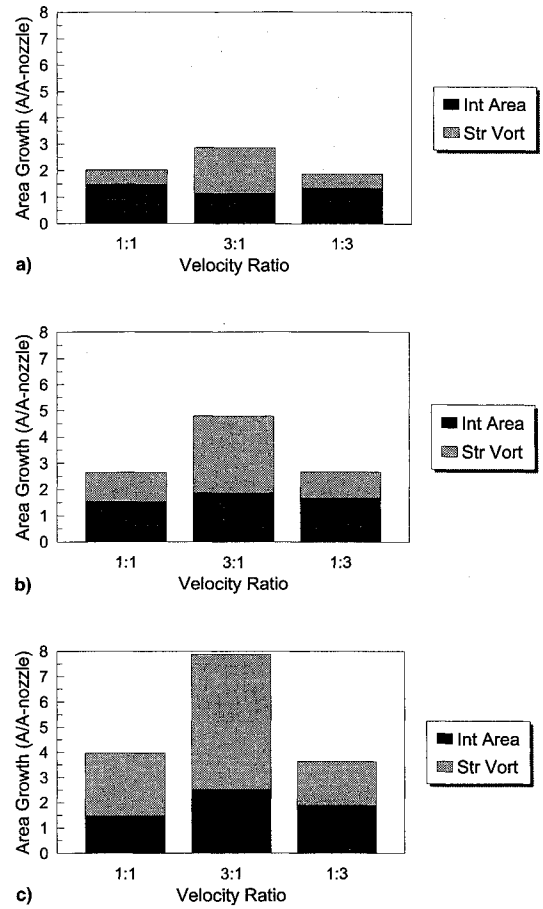

Fig. 12 Comparison of absolute contributions of interfacial contact area and streamwise vorticity to total mixing for the 10-deg ramp angle nozzle. x/D = a) 1, b) 2, and c) 3.

total image size is 288 × 192 (=55,296) pixels, while the nozzle exit area is represented by approximately 1100 pixels. The graphs show a general trend of increasing inner jet area with increasing distance downstream and also with increasing streamwise vorticity. Figure 11a shows that the inner jet from nozzle 3 grows to approximately 30 times its original size. While these graphs corroborate the trends in the images previously shown, these inner jet spread region estimates should be considered nominal estimates, particularly at the furthest downstream locations.

One of the objectives of the present study is to separate the contributions to overall mixing due to the increase in interfacial area and the streamwise vorticity generated by the lobed nozzles. The difference in the spread inner jet area between nozzle 2 (0-deg ramp) and the baseline nozzle provides the contribution to total mixing due to the increase in interfacial area. The difference in the spread inner jet area between nozzle 1 (10-deg ramp) and the baseline nozzle provides the contribution to mixing due to both interfacial area and streamwise vorticity. The contribution due to streamwise vorticity alone is found by subtracting the two. Using the data of Fig. 11, these separate effects on mixing enhancement can be found and their relative contributions calculated. Table 3 shows the results for several x/D locations for nozzle 1. The x/D locations of 5 and 7 are not shown because the area calculations for these locations have the most uncertainty due to some clipping of the images by the laser sheet. At x/D = 1 and a velocity ratio of 3:1, the contribution to overall mixing due to streamwise vorticity is greater than the contribution of the interfacial area. Moving downstream, the contribution from the interfacial area decreases slightly, while the streamwise vorticity enhancement increases. This is consistent with previous work[15,22] showing that the streamwise vortices grow first, then break down downstream, thereby increasing turbulence levels and mixing. As the vortices go through the processes of stretching, pairing, and tearing, mixing increases. For the velocity ratio of 1:1, the interfacial area provides a much larger fraction of the mixing than the streamwise vorticity at x/D = 1. The same trends as for the 3:1 velocity ratio are evident moving downstream. However, the fractional contribution due to interfacial area decreases, hence, that due to streamwise vorticity increases at a much faster rate. Since the Kelvin–Helmholtz effect is minimized for this case, the streamwise vortices are the dominant structures in the flow. As they interact downstream, their mixing effects care more

prevalent. The results for the 1:3 velocity ratio are similar to the previous two cases. The relative contributions to mixing at $x/D = 1$ are in approximately the same proportions as for the 1:1 case, but the change in proportions moving downstream is about the same as the 3:1 case.

Figure 12 shows the data of Fig. 11 and Table 3 for the three velocity ratios. The bar graphs show the total mixing for nozzle 1 at three different locations downstream, but with the interfacial area and streamwise vorticity contributions shaded differently. Even though the fraction of mixing due to the interfacial area decreases as velocity ratio increases, the total amount of mixing due to interfacial area is still significant, contributing at least 30% to the total mixing in all cases. Comparing different velocity ratios for each x/D location, there is a distinct increase in total mixing as velocity ratio increases and the percentage of enhancement due to streamwise vorticity increases. This is in agreement with Manning's[24] results, except Manning did not discuss any effect due to downstream distance.

IV. Conclusions

Flow visualizations using a passive scalar have been performed to explore mixing enhancement in an axisymmetric coaxial jet with an inner, lobed mixer. Four different central jet geometries, three lobed-mixer nozzles and a circular nozzle, were used to investigate three different mixing mechanisms involved, namely the increased interfacial contact area, the streamwise vorticity, and the inner/outer velocity ratio. Instantaneous and average images showed the pronounced effect of the Kelvin–Helmholtz roll-up on mixing even with the presence of very strong streamwise vortices. The fraction of mixing enhancement due to streamwise vorticity (relative to mixing enhancement due to increased interfacial contact area) was found to increase as velocity ratio increased. In addition, this fraction increased with downstream distance. Overall, the lobed mixer nozzle with the largest ramp angle of 20 deg (strongest streamwise vortices), produced the highest mixing at all velocity ratios.

Acknowledgments

This project was funded under Air Force Office of Scientific Research G-F49620-92-J-0224 with J. M. Tishkoff and W. M. Roquemore as Contract Monitors. The authors would also like to thank W. M. Roquemore for many helpful discussions. The authors would additionally like to thank the support staff of the Aeronautical and Astronautical Research Laboratory at Ohio State University, Columbus, Ohio, for their cooperation.

References

[1]Paterson, R. W., "Turbofan Forced Mixer-Nozzle Internal Flowfield," NASA CR 3492, 1982.

[2]Paterson, R. W., "Turbofan Mixer Nozzle Flow Field—A Benchmark Experimental Study," *Journal of Engineering for Gas Turbines and Power*, Vol. 106, July 1984, pp. 692–698.

[3]Povinelli, L. A., Anderson, B. H., and Gerstenmaier, W., "Computation of Three Dimensional Flow in Turbofan Mixers and Comparison with Experimental Data," AIAA Paper 80-0227, Jan. 1980.

[4]Frost, T. H., "Practical Bypass Mixing Systems for Fan Jet Aero Engines," *Aeronautical Quarterly*, Vol. 17, May 1966, pp. 141–161.

[5]Anderson, B., Povinelli, L., and Gerstenmaier, W., "Influence of Pressure Driven Secondary Flows on the Behavior of Turbofan Forced Mixers," AIAA Paper 80-1198, June 1980.

[6]Birch, S. F., Paynter, G. C., Spalding, D. B., and Tatchell, D. G., "An Experimental and Numerical Study of the 3-D Mixing Flows of a Turbofan Engine Exhaust System," AIAA Paper 77-0204, Jan. 1977.

[7]Blackmore, W. L., and Thompson, C. E., "3-D Viscous Analysis of Ducts and Flow Splitters," AIAA Paper 81-0277, Jan. 1981.

[8]Crouch, R. W., Coughlin, C. L., and Paynter, G. C., "Nozzle Exit Flow Profile Shaping for Jet Noise Reduction," AIAA Paper 76-0511, July 1976.

[9]Head, V. L., Povinelli, L. A., and Gerstenmaier, W. H., "Hot-Flow Tests of a Series of 10-Percent Scale Turbofan Forced Mixing Nozzles," NASA TP 2268, 1984.

[10]Kozlowski, H., and Kraft, G., "Experimental Evaluation of Exhaust Mixers for an Energy Efficient Engine," AIAA Paper 80-1088, June 1980.

[11]Kuchar, A. P., and Chamberlin, R., "Scale Model Performance Test Investigation of Exhaust System Mixers for an Energy Efficient Engine (E^3) Propulsion System," AIAA Paper 80-0229, Jan. 1980.

[12]Shumpert, P. K., "An Experimental Model Investigation of Turbofan Engine Internal Exhaust Gas Mixer Configurations," AIAA Paper 80-0228, Jan. 1980.

[13]Packman, A. B., Kozlowski, H., and Gutierrez, O., "Jet Noise Characteristics of Unsuppressed Duct Burning Turbofan Exhaust Systems," AIAA Paper 76-0149, July 1976.

[14]Povinelli, L. A., and Anderson, B. A., "Investigation of Mixing in a Turbofan Exhaust Duct, Part II: Computer Code Application and Verification," *AIAA Journal*, Vol. 22, No. 4, 1984, pp. 518–525.

[15]Werle, M. J., Paterson, R. W., and Presz, W. M., Jr., "Flow Structure in a Periodic Axial Vortex Array," AIAA Paper 87-0610, Jan. 1987.

[16]Presz, W., Jr., Gousy, R., and Morin, B., "Forced Mixer Lobes in Ejector Designs," AIAA Paper 86-1614, June 1986.

[17]Skebe, S. A., McCormick, D. C., and Presz, W. M., Jr., "Parameter Effects on Mixer-Ejector Pumping Performance," AIAA Paper 88-0188, Jan. 1988.

[18]Malecki, R., Mityas, S., and Lord, W., "Navier-Stokes Analysis of an Ejector and Mixer-Ejector Operating at Pressure Ratios in the Range 2–4," AIAA Paper 90-2730, July 1990.

[19]Tillman, T. G., Patrick, W P., and Paterson, R. W., "Enhanced Mixing of Supersonic Jets," AIAA Paper 88-3002, July 1988.

[20]McVey, J. B., "Observation of the Effect of Streamwise Vorticity on the Spreading of Flames in High Speed Flow," *Combustion Science and Technology*, Vol. 60, 1988, pp. 447–451.

[21]McVey, J. B., and Kennedy, J., "Flame Propagation Enhancement Through Streamwise Vorticity Stirring," AIAA Paper 89-0619, Jan. 1989.

[22]Eckerle, W. A., Sheibani, H., and Awad, J., "Experimental Measurement of the Vortex Development Downstream of a Lobed Forced Mixer," American Society of Mechanical Engineers Paper 90-GT-27, 1990.

[23]Barber, T., Paterson, R. W., and Skebe, S. A., "Turbofan Forced Mixer Lobe Flow Modeling. Part I. Experimental and Analytical Assessment," NASA CR 4147, 1988.

[24]Manning, T. A., "Experimental Studies of Mixing Flows with Streamwise Vorticity," M.S. Thesis, Massachusetts Inst. of Technology, Cambridge, MA, 1991.

[25]Elliott, J. K., Manning, T. A., Qiu, Y. J., Greitzer, E. M., Tan, C. S., and Tillman, T. G., "Computational and Experimental Studies of Flow in Multi-Lobed Forced Mixers," AIAA Paper 92-3568, July 1992.

[26]McCormick, D. C., "Vortical and Turbulent Structure of Planar and Lobed Mixer Free-Shear Layers," Ph.D. Dissertation, Univ. of Connecticut, Storrs, CT, 1992.

[27]McCormick, D. C., and Bennett, J. C., Jr., "Vortical and Turbulent Structure of a Lobed Mixer Free-Shear Layer," AIAA Paper 93-0219, Jan. 1993.

[28]Presz, W. M., Jr., Reynolds, G., and McCormick, D., "Thrust Augmentation Using Mixer-Ejector-Diffuser Systems," AIAA Paper 94-0020, Jan. 1994.

[29]Tennekes, H., and Lumley, J. L., "A First Course in Turbulence," Massachusetts Inst. of Technology Press, Cambridge, MA, 1972, Chap. 4.

[30]Champagne, F. H., and Wygnanski, I. J., "An Experimental Investigation of Coaxial Turbulent Jets," *International Journal of Heat and Mass Transfer*, Vol. 14, 1971, pp. 1445–1464.

[31]Dahm, W. J. A., Frieler, C. E., and Tryggvason, G., "Vortex Structure and Dynamics in the Near Field of a Coaxial Jet," *Journal of Fluid Mechanics*, Vol. 241, 1992, pp. 371–402.

[32]Ko, N. W., and Au, H., "Coaxial Jets of Different Mean Velocity Ratios," *Journal of Sound and Vibration*, Vol. 100, No. 2, 1985, pp. 211–232.